Iranian Journal of Chemical Engineering

Journal Homepage: www.ijche.com

pISSN: 1735-5397
eISSN: 2008-2355

CFD Simulation of Hydrogen Sulfide (H_2S) Removal from Crude Oil Through an Optimized Cold Stripping Process in a Microchannel

Faezeh Mohammadi [1] *, ***Ebrahim Ebrahimi*** [2]

[1] *Department of Chemical Engineering, Ker. C., Islamic Azad University, Kermanshah, Iran*
[2] *Department of Mechemical Engineering, Ker. C., Islamic Azad University, Kermanshah, Iran*

ARTICLE INFO

Article type:
Research article

Article history:
Received: 2025-09-15
Revised: 2025-10-27
Accepted: 2025-11-20
Available online: 2025-11-22

Keywords:
CFD simulation,
H_2S removal,
Cold stripping,
Microchannel,
Crude oil

ABSTRACT

The present study numerically investigates the removal of hydrogen sulfide (H_2S) from crude oil using natural gas as a stripping medium in a T-junction microchannel through three-dimensional computational fluid dynamics (CFD) simulations. The microchannel geometry was adapted from a previously reported experimental configuration and further optimized to reduce natural gas consumption and operating temperature. The Volume of Fluid (VOF) model coupled with the SIMPLE algorithm was implemented in ANSYS Fluent to simulate the gas–liquid two-phase flow and evaluate mass transfer characteristics. Simulations were conducted for the gas flow rates of 200–1200 mL/min and oil temperatures in the range of 20–40 °C. The results showed that the H_2S removal efficiency increased with crude oil temperature and gas flow rate but decreased with higher oil flow rates. The predicted efficiencies were between 65.7% and 77.8%, and in close agreement with experimental data (maximum relative error: 5.6%). The cold-stripping configuration achieved high desulfurization performance even at low gas temperatures (about 18 °C) while reducing gas consumption by nearly one-third compared with conventional units. This study proposes validated correlations and optimized operating parameters for the efficient desulfurization of sour crude oil using a microchannel-based cold stripping process.

DOI: 10.22034/ijche.2025.547421.1573 URL: https://www.ijche.com/article_234720.html

1.Introduction

Hydrogen sulfide (H_2S) is a highly toxic and corrosive gas frequently encountered in crude oil and natural gas streams. Its presence not only causes severe corrosion in pipelines and refinery equipment but also poses serious

*Corresponding author: Faezehmohammadi@iau.ac.ir

environmental and health risks [1-3]. The removal of H_2S prior to transportation or refining is therefore a critical requirement for both environmental protection and process safety [4,5]. Crude oils containing more than 6 ppm of dissolved H_2S are considered corrosive due to the formation of iron sulfide scales on tank walls and pipelines, leading to equipment failure and operational hazards [6].

Over the past decades, several physical, chemical, and biological methods, including amine absorption, use of chemical scavengers, membrane separation, adsorption on solid sorbents, and physical stripping using gases such as nitrogen or natural gas, have been developed for the desulfurization of sour crude oil [7-11]. While chemical processes can achieve near-complete sulfur removal, they are typically expensive, energy-intensive, and difficult to regenerate. In contrast, physical cold stripping has emerged as a promising alternative due to its lower energy demand, simple operation, and reduced environmental impact [12,13].

Recent advancements in microfluidic technologies have opened up new opportunities for process intensification in mass transfer operations [14-17]. Microchannels, characterized by their high surface-to-volume ratios, enhanced mixing, and short residence times, offer significant advantages for gas–liquid contact and stripping applications [18-21]. Several researchers have reported the improved performance of H_2S and CO_2 removal in microstructured devices [22-26]. Almasvandi et al. (2016) experimentally demonstrated the H_2S removal efficiencies of 65.7–77.8% in a T-junction microchannel, while Pan et al. (2015) achieved nearly 99.8% removal using a tube-in-tube microreactor with N-MDEA solvent [27,28]. In the last few years, numerous studies have further explored CFD-based modeling of microchannel desulfurization and multiphase flow [29-31]. Yao et al. (2021) analyzed interfacial dynamics in gas–liquid microchannels and developed new correlations for Sherwood and Nusselt numbers [22]. Chen et al. (2022) investigated CO_2 and H_2S mass transfer in microreactors using ANSYS Fluent, and reported that increasing slug flow improves the absorption efficiency by up to 20% [29]. Davidy et al. (2023) simulated H_2S removal using ionic liquids and graphene oxide membranes, and demonstrated superior absorption at reduced regeneration energy [24]. Li et al. (2023) applied deep learning-assisted CFD to predict H_2S removal rates in deep eutectic solvent systems, and showed strong agreement with experimental data [30]. More recently, Tran et al. (2024) developed a CFD-based design optimization for high-gravity rotating packed beds to simultaneously remove H_2S and CO_2 with efficiencies exceeding 90% [31]. These recent findings highlight the growing role of CFD in optimizing desulfurization processes. Despite these advancements, limited work has been done on the cold stripping of H_2S using natural gas in crude oil systems under optimized operating conditions. Moreover, no prior research has provided a validated CFD-based correlation linking operational parameters (temperature, flow rates, and geometry) to the efficiency of desulfurization.

The present study aims to fill this research gap by performing the three-dimensional CFD simulations of H_2S removal from crude oil using the Volume of Fluid (VOF) method and the SIMPLE algorithm to couple pressure–velocity fields. The study adopts the geometry, which has been experimentally validated by Almasvandi et al. (2016), and introduces an optimized configuration to minimize gas consumption and energy requirements while

maintaining high separation efficiency. A mesh independence test and sensitivity analysis were conducted to ensure numerical accuracy. The results are validated against published experimental data, and new correlations are proposed for predicting the H_2S mass transfer efficiency in T-junction microchannels. The novelty of this work lies in its CFD-based assessment of cold stripping performance in microchannels, the optimization of design and operating parameters for the higher H_2S removal efficiency, and the development of a general modeling approach for future desulfurization applications.

2. Methodology and Numerical Modeling

2.1. Geometry and Mesh Generation

The microchannel geometry was designed based on the experimental configuration reported by Almasvandi et al. (2016) and optimized toreduce gas consumption and operating temperature. The main part of the experimental setup was a T-shaped microchannel made of plexiglass and a glass microtube with an inner diameter of 0.9 mm and a length of 500 mm. Figure 1 presents the schematic configuration of the simulated microchannel used in this study.

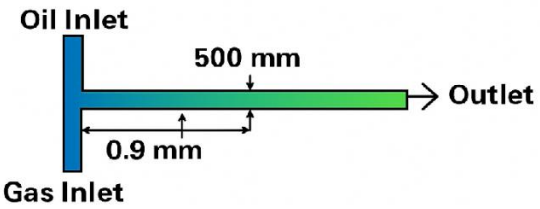

Figure 1. Schematic of the microchannel simulated in this study.

The horizontal main channel had a length of 500 mm and an inner diameter of 0.9 mm, while the vertical inlet branch for the gas phase had a length of 100 mm and the same diameter. The outlet section was connected to a cylindrical separator chamber with the diameter of 63 mm and the height of 400 mm. The geometry was constructed using Gambit 2.4.6, and the grid was generated using tetrahedral–hybrid elements with local refinement near the T-junction to capture the interface behavior.

A mesh independence test was conducted using three mesh densities (coarse: 0.2 mm, medium: 0.1 mm, fine: 0.05 mm). The computed H2S removal efficiency differed by less than 2% between the medium and fine meshes; Therefore, the medium grid (approximately 1.2×10^6 cells) was selected as the one with the optimal balance between accuracy and computational cost.

2.2. Model Assumptions and Governing Equations

The flow was assumed to be laminar, isothermal, and incompressible, which is consistent with the low Reynolds number (Re < 1000) and small hydraulic diameter of the microchannel. The oil phase was modeled as a Newtonian liquid, while the gas phase (natural gas) was treated as a compressible mixture of methane with trace H_2S.

The Volume of Fluid (VOF) approach was used to capture the gas–liquid interface dynamics. The continuity, momentum, and species transport equations were solved simultaneously in transient mode using the finite volume method in ANSYS Fluent 2022R1. The pressure–velocity coupling was handled by the SIMPLE algorithm, with a time-step size of 10^{-3} s, ensuring stable convergence.

The second-order upwind scheme was used for the spatial discretization of the momentum and energy equations, while the pressure term was treated using the PRESTO! scheme. The volume fraction was solved using the geometric reconstruction approach to accurately trace the interface.

Convergence was assumed when the scaled residuals of continuity, momentum, and species equations dropped below 10^{-6}. Simulations were run until steady periodic conditions were achieved.

Three-dimensional CFD modeling involves solving the unsteady form of the Navier–Stokes conservation equations, which can be expressed for any scalar quantity φ, as [32]:

$$\frac{\partial}{\partial t}(\alpha\rho\varphi) + \nabla(\alpha\rho\vec{\upsilon}\varphi) = \nabla(\Gamma_{\varphi}\nabla\varphi) + S_{\varphi} \quad (1)$$

where ρ is the mixture density, α is the phase volume fraction, ν is the velocity vector, Γ is the diffusion coefficient, and S_{φ} represents the source term. The physical properties of the liquid and gas phases, including density, viscosity, and diffusivity, were defined in the materials section of Fluent. The properties of the mixture were computed using standard mixing rules. For the mass penetration coefficient, the dilute estimation option is used and the penetration coefficient of all compounds has been introduced to the software.

In the multiphase flow involving the interfacial mass transfer, the mass fraction of each species (X_i) in the liquid phase is determined according to the following equation [32]:

$$\frac{\partial(\alpha_l\rho_l X_i^l)}{\partial t} + \nabla.\left(\alpha_l\rho_l\vec{v}_l X_i^l\right) = -\nabla.\alpha_l\vec{J}_i^l + \alpha_l R_i^l \quad (2)$$

here, R_i represents the net production rate of species i due to chemical reactions. $\vec{J_i}$ is the diffusive flux of species i arisen from the concentration gradient in the liquid phase. The continuity equation of the gas-liquid two-phase flow in the Fluent software is solved only for gas (the second phase), which is as follows:

$$\frac{\partial(\alpha_g\rho_g)}{\partial t} + \nabla.\left(\alpha_g\rho_g\vec{v}_g\right) = \dot{m}_{g\to liq} - \dot{m}_{liq\to g} \quad (3)$$

The volume component equation (α) is solved only for the second phase and not for the first phase. In fact, the volume component of the first phase (α_{aq}) is obtained based on the following equation:

$$\alpha_{or} + \alpha_{aq} = 1 \quad (4)$$

2.3. Boundary Conditions

The boundary conditions applied in this simulation are summarized as follows. The oil inlet was defined as a velocity inlet, with the flow rate ranging from 50 to 120 mL/min, the temperature of between 20 and 40 °C, and an initial concentration of 50 ppm of H_2S. The gas inlet was also set as a velocity inlet, with flow rates varying from 200 to 1200 mL/min, a fixed temperature of 28 °C, and an H_2S mole fraction of 0.0002. At the outlet, a pressure outlet boundary condition was imposed at 1 atm, with zero-gradient conditions for all scalar variables. Table 1 summarizes the boundary conditions applied in this simulation.

Table 1.
Boundary conditions

Boundary Zone	Type
Gas Inlet	Velocity Outlet
Liquid Inlet	Velocity Inlet
Outlet	Pressure outlet
Other walls	Wall

The channel walls were treated as no-slip boundaries with zero mass flux. The gravitational acceleration of –9.81 m/s² was applied along the vertical axis, and the reference pressure was defined at the outlet.

2.4. Mass Transfer and Interfacial Forces

The interfacial mass transfer between the gas and liquid phases was modeled using the following equation:

$$N_i = K_L a(C_i^* - C_i) \quad (5)$$

where N_i is the molar flux, K_L is the liquid-side mass transfer coefficient, a is the interfacial area per unit volume, and C_i^* and C_i denote the equilibrium and bulk concentrations of H_2S respectively. The interfacial forces considered in the momentum equation included drag, lift, virtual mass, and surface tension, as expressed in Fluent's two-phase VOF formulation [32]:

$$F = F_d + F_l + F_{vm} + F_\sigma \quad (6)$$

where F_d, F_l, F_{vm}, and F_σ denote the drag, lift, virtual mass, and surface tension forces respectively. These terms are included in the momentum balance to represent the gas–liquid interfacial interactions within the microchannel. These additions ensure a more comprehensive and physically consistent representation of the two-phase flow system.

3. Results and Discussion

3.1. Flow Hydrodynamics and Phase Distribution

The simulated velocity and phase contours within the T-junction microchannel revealed a stable laminar flow pattern with clearly defined gas–liquid interfaces. Figure 2 illustrates the gas-phase distribution along the microchannel. As expected, at the outlet section, the gas and liquid phases form a distinct interface, through which mass transfer occurs. During the stripping process, H_2S is transferred from the liquid phase to the gas phase due to concentration gradients. The periodic formation of dispersed gas bubbles was observed at the junction, which were subsequently transported downstream, creating alternating gas–liquid slug segments. The maximum velocity appeared along the channel centerline (~0.1 m/s), while the velocity near the wall approached zero, confirming the characteristics of the fully developed laminar flow.

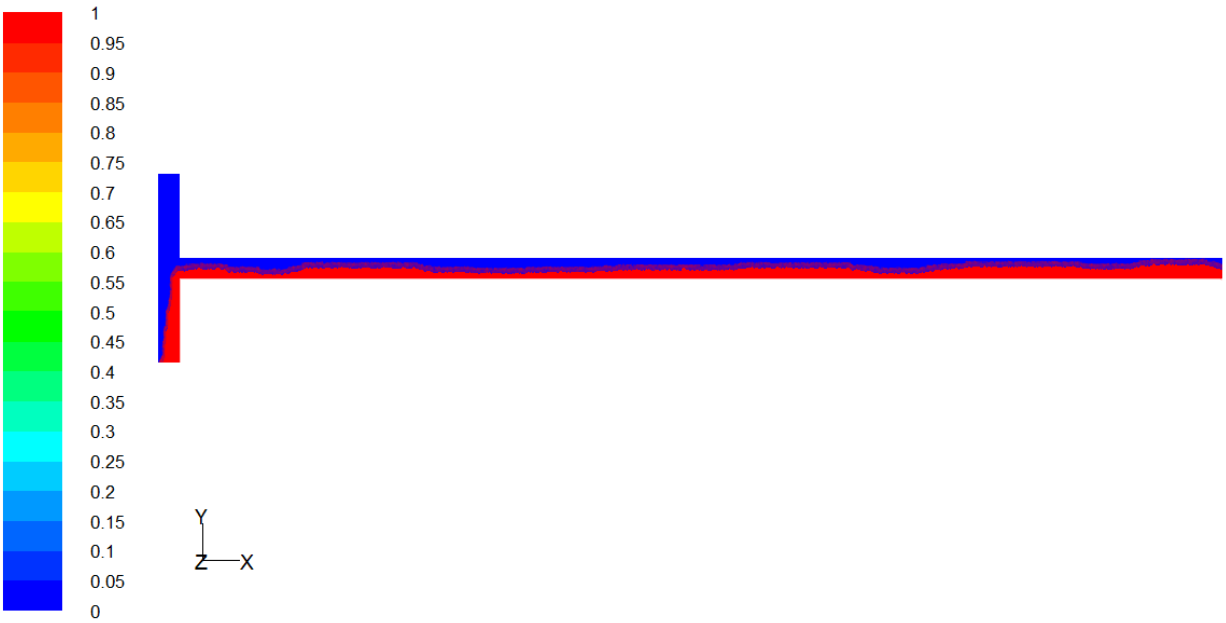

Figure 2. Contour of the gas phase in the microchannel in section Z=0.

Figure 3. shows the velocity contour in the microchannel. The velocity contour shows that the velocity at the center of the tube has its maximum value and is about 0.1 m/s, but the velocity at the wall of the microchannel is zero.

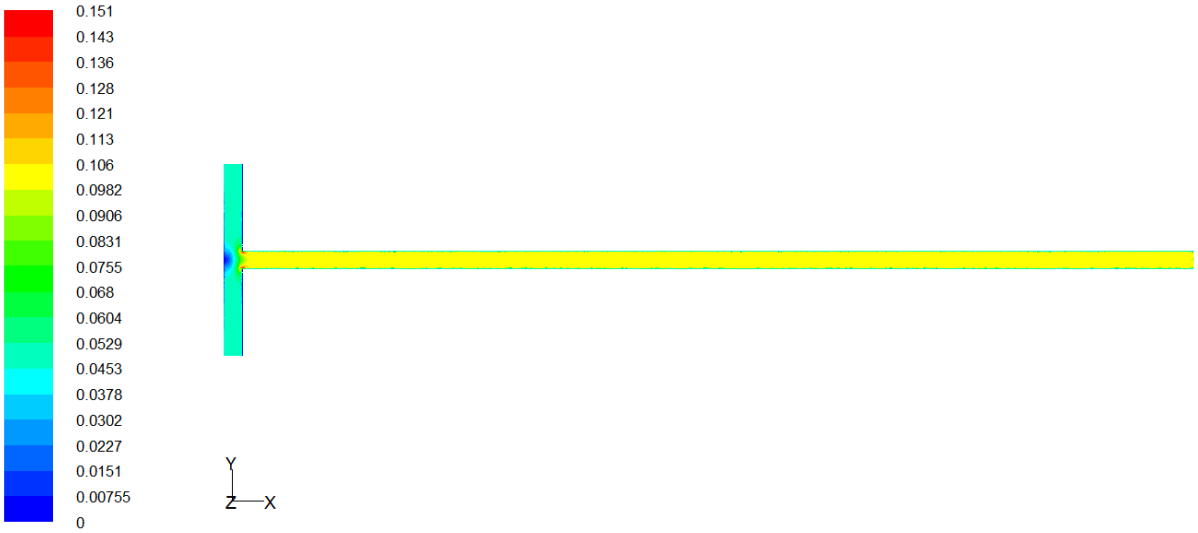

Figure 3. Velocity contour in the microchannel at the Z=0 cut.

Figures 4 and 5 show the pressure contour and the velocity vector in the microchannel respectively. Figure 4 shows that the flow of the liquid and the gas phase move towards the outlet after the collision at the intersection of the microchannel. The velocity in the center of the microchannel has its maximum value and is about 0.1 m/s.

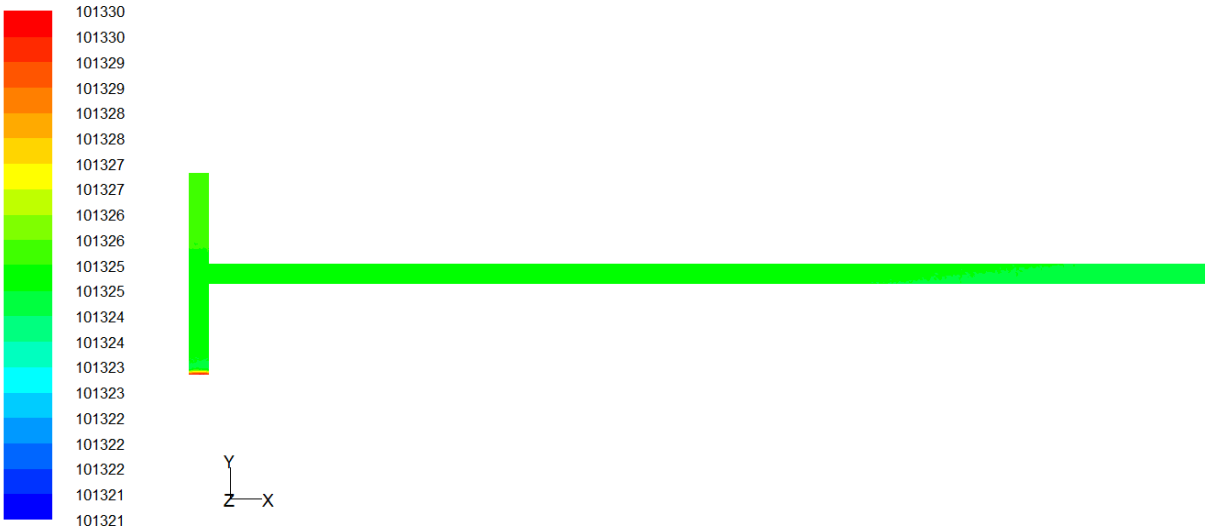

Figure 4. Pressure contour in the microchannel at the Z=0 cut.

The interfacial area between the oil and gas phases played a crucial role in determining the mass transfer rate of H_2S. The VOF model successfully captured the dynamic deformation of the interface and the bubble elongation during the flow, which directly affected the rate of the H_2S desorption from the liquid phase into the gas phase. These hydrodynamic results are in agreement with the observations of Rahimi et al. (2017) and Kakavandi et al. (2016), who demonstrated that bubble size and frequency dominate the mass-transfer performance in microchannel contactors [19,20].

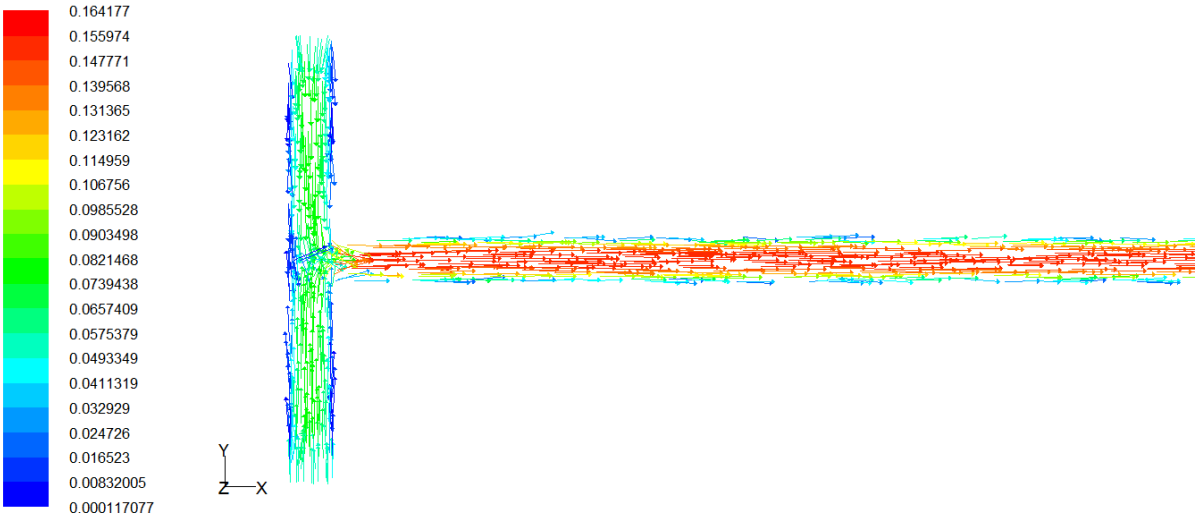

Figure 5. Velocity vector in the microchannel at slice Z=0.

3.2. Effect of Temperature on H_2S Removal Efficiency

In this study, the H_2S mass transfer efficiency was employed as a key indicator to evaluate its separation behavior when separated from crude oil, which was calculated using the following equation:

$$\eta = \frac{C_{in,H_2S} - C_{out,H_2S}}{C_{in,H_2S}} \times 100 \quad (7)$$

where C_{in} and C_{out} are the volume fractions of H_2S at the gas inlet and outlet respectively. Figure 6 shows the relationship between the crude-oil temperature and H_2S removal efficiency at the constant flow rates of 85 mL/min (oil) and 700 mL/min (gas). The CFD predictions indicate that efficiency increases from 65.7% at 20°C to 77.8% at 40°C, which is in excellent agreement with the experimental data reported by Almasvandi et al. (2016) (the maximum deviation < 5.6%).

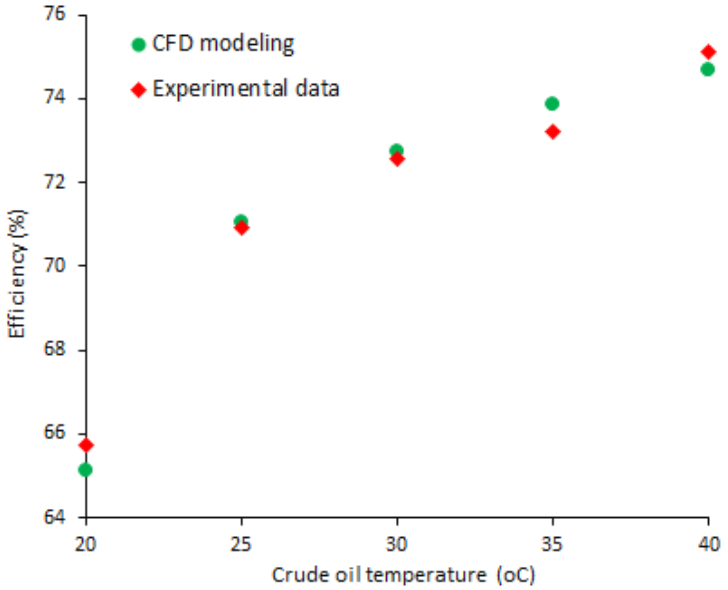

Figure 6. Effect of the crude oil temperature on the efficiency of H_2S removal in terms of microchannels in section Z=0.

This trend can be attributed to the increased diffusion coefficient and reduced viscosity of the oil at higher temperatures, enhancing the interfacial mass transfer. Furthermore, a rise in temperature promotes desorption by reducing the solubility of H_2S in the oil phase, which is consistent with Henry's law. Similar thermal effects on H_2S removal have also been reported by Hazrati et al. (2014). More recently, it was observed that the gas desulfurization efficiency increased by 10–15% for each 10 °C rise in temperature in microreactor simulations [5,29].

3.3. Effect of the Gas Flow Rate

Figure 7 presents the effect of the natural gas flow rate (200–1200 mL/min) on the H_2S removal efficiency at a fixed oil flow rate of 70 mL/min and temperature of 25°C. The efficiency increased rapidly with gas flow rate up to 800 mL/min, beyond which it approached an asymptotic limit.

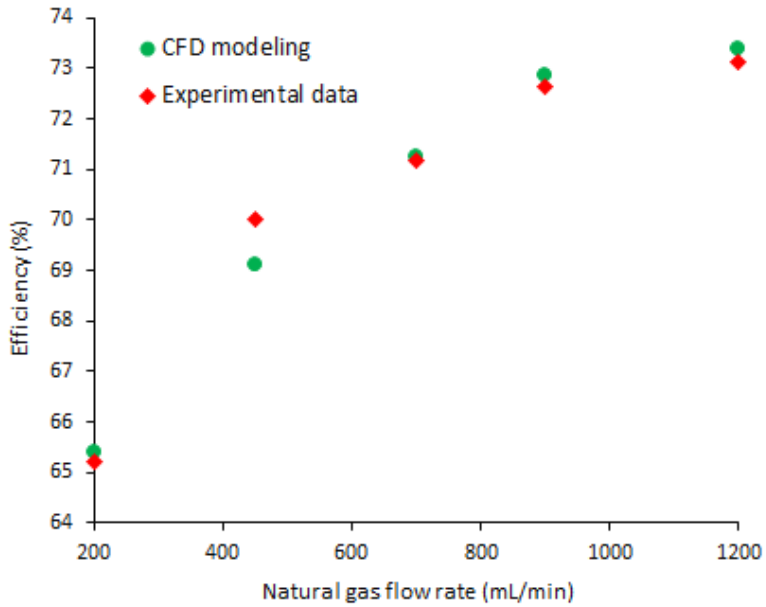

Figure 7. Effect of the gas flow rate on the H_2S removal efficiency in terms of microchannel in section Z=0.

At higher gas flow rates, the enhanced interfacial area and turbulence intensify the stripping process, compensating for the reduced residence time. This behavior agrees with the studies of Pan et al. (2015) and Zhang et al. (2021), who also observed diminishing returns in efficiency beyond a critical gas–liquid ratio due to the coalescence of bubbles and the reduced contact time [22,28].

Compared to in previous works, the optimized geometry used in this study achieved similar efficiency levels but with 30–35% lower gas consumption and operating temperatures 10–15°C lower than those reported by Pan et al. (2015). This demonstrates the energy-saving advantage of cold stripping in microchannels [28].

3.4. Model Accuracy and Limitations

The absolute relative error (ARE%) for H_2S removal efficiency values is defined in equation (8) as follows:

$$ARE\,\% = \left| \frac{(measured\ \text{value} - predicted\ \text{value})}{measured\ \text{value}} \right| \times 100 \quad (8)$$

The comparison between CFD predictions and laboratory data revealed good agreement with a maximum relative error of 5.6%. Minor discrepancies at higher gas flow rates may arise from simplified assumptions such as considering physical properties as constant and ignoring the possible slug-to-annular flow transition. Future work will include more complex flow regimes and temperature-dependent property correlations.

4. Conclusion

In this study, a three-dimensional CFD simulation was conducted to analyze the removal of hydrogen sulfide (H_2S) from crude oil through an optimized cold stripping process in a T-junction microchannel using natural gas as the stripping medium. The VOF model combined with the SIMPLE algorithm was applied in ANSYS Fluent to simulate the gas–liquid two-phase flow and predict the mass transfer performance. The numerical results demonstrated that the H_2S removal efficiency increased with the crude oil temperature and gas flow rate but decreased with higher oil flow rates. The maximum removal efficiency of 77.8% was achieved at the oil temperature of 40 °C, gas flow rate of 700 mL/min, and oil flow rate of 85 mL/min, which was in close agreement with experimental data (maximum relative error = 5.6%). The optimized microchannel design provided similar efficiency to previous experimental studies while reducing gas consumption by approximately 30–35% and operating temperature by 10–15 °C, confirming its energy-saving potential. The study's main contribution lies in developing a validated CFD framework and proposing new correlations for predicting the H_2S mass transfer efficiency in microchannel-based cold stripping systems. The model assumptions—including laminar, isothermal, and incompressible flow with Newtonian fluid behavior—represent reasonable simplifications for the studied operating conditions but may limit applicability to higher Reynolds numbers or temperature-dependent systems. Future work will focus on extending this model to consider temperature-dependent physical properties, non-Newtonian behavior of oil, and reactive or catalytic cold-stripping configurations, with the aim of further increasing desulfurization efficiency and its industrial applicability.

References

[1] Zheng D, Jiang Z, Shi J, Wang Y, Liu Z (2020) Experimental analysis of the effect of nitrogen gas on the H_2S stripping process during the pigging operation of a long crude oil pipeline. Case Studies in Thermal Engineering 22: 100741. https://doi.org/10.1016/j.csite.2020.100741

[2] Mohammadi F, Moradpour N, Azimi N, Ebrahimi E (2024) Feasibility of the purification of pharmaceuticals from aqueous solutions using carbon nanotubes in the presence of oxidizers. Iranian Journal of Chemical Engineering (IJChE) 21(2): 43–55. https://doi.org/10.22034/ijche.2024.443106.1523

[3] Mohammadi F, Jan Amiri R, Azimi N, Salimi F (2024) Achieving optimal conditions of membrane bioreactors for dairy industry wastewater treatment. Iranian Journal of Chemical Engineering (IJChE) 21(3): 49–65. https://doi.org/10.22034/ijche.2024.457926.1533

[4] Husein MM, Patruyo L, Pereira-Almao P, Nassar NN (2010) Scavenging $H_2S(g)$ sorption from oil phases by means of ultradispersed sorbents. Journal of Colloid and Interface Science 342: 253–260. https://doi.org/10.1016/j.jcis.2009.10.059

[5] Hazrati N, Abdouss M, Vahid A, Miran

Beigi AA, Mohammadalizadeh A (2014) Removal of H_2S from crude oil via stripping followed by adsorption using ZnO/MCM-41 and optimization of parameters. International Journal of Environmental Science and Technology 11: 997–1006. https://doi.org/10.1007/s13762-013-0465-z

[6] Ebnali M, Shahbazian M, Jazayerirad H (2018) Artificial Intelligence for inferential control of crude oil stripping process. Iranian Journal of Oil Gas Science and Technology 7: 70–92. https://doi.org/10.22050/IJOGST.2017.54928.1337

[7] Elshiekh TM, Elmawgoud HA, Khalil SA, Alsabagh AM (2016) Optimum injection dose rate of hydrogen sulfide scavenger for treatment of petroleum crude oil. Egyptian Journal of Petroleum 25: 75–78. https://doi.org/10.1016/j.ejpe.2015.03.015

[8] Elshiekh TM, Elmawgoud HA, Khalil SA, Alsabagh AM (2015) Simulation for estimation of hydrogen sulfide scavenger injection dose rate for treatment of crude oil. Egyptian Journal of Petroleum 24: 469–474. https://doi.org/10.1016/j.ejpe.2014.12.002

[9] Li X, Zhou W, Liu J, Feng L (2023) Intelligent modeling of hydrogen sulfide removal by deep eutectic solvents for environmental protection. Separation and Purification Technology 315: 123621. https://doi.org/10.1016/j.seppur.2023.123621

[10] Tran LT, Le TM, Nguyen TM, Tran QT, Le XD, Pham MQ, Lam VT, Do MV (2024) Simultaneous removal efficiency of H_2S and CO_2 by high-gravity rotating packed bed: Experiments and simulation. Chem. https://doi.org/10.1515/chem-2020-0187

[11] Zhang L, et al. (2008) Chemical and biological technologies for hydrogen sulfide emission control in sewer systems: a review. Water Research. https://doi.org/10.1016/j.watres.2007.07.013

[12] Brinkmann WLF, Santos UDM (2010) The emission of biogenic hydrogen sulfide from Amazonian floodplain lakes. Tellus 26(1–2): 261–267. https://doi.org/10.1111/j.21533490.1974.tb01975.x

[13] Lee J, Kumar R (2013) Laboratory study of hydrogen sulfide removal in slug flows in a high-pressure crude oil loop. Journal of Petroleum Science and Engineering 103: 72–79. https://doi.org/10.1016/j.petrol.2013.01.009

[14] Basiri M, Rahimi M, Mohammadi F (2015) Investigation of liquid–liquid two-phase flow pattern in microreactors for biodiesel production. Iranian Journal of Chemical Engineering 12(3): 45–53. https://doi.org/20.1001.1.17355397.2015.12.3.3.3

[15] Rahimi M, Mohammadi F, Basiri M, Parsamoghadam MA, Masahi MM (2016) Transesterification of soybean oil in four-way micromixers for biodiesel production using a cosolvent. Iranian Journal of Chemical Engineering 63: 123–131. https://doi.org/10.1016/j.jtice.2016.04.023

[16] Mohammadi F, Rahimi M, Parvareh A, Feyzi M (2018) Biodiesel production from soybean oil using ionic liquid as a catalyst in a microreactor. Iranian Journal of Chemical Engineering 15(2): 45–53. https://doi.org/20.1001.1.17355397.2018.15.1.7.4

[17] Mohammadi F, Rahimi M, Parvareh A, Feyzi M (2017) Stimulation of magnetic nanoparticles to intensify transesterification of soybean oil in micromixers for biodiesel production. Chemical Engineering and Processing 117: 200–208. https://doi.org/10.1016/j.cep.2017.10.007

[18] Yin Y, Guo R, Zhu C, Fu T, Ma Y (2020) Enhancement of gas–liquid mass transfer in

microchannels by rectangular baffles. Separation and Purification Technology 236: 116360. https://doi.org/10.1016/j.seppur.2019.116306

[19] Rahimi M, Azimi N, Parsamoghadam MA, Rahimi A, Masahy MM (2017) Mixing performance of T-, Y-, and oriented Y-micromixers with spatially arranged outlet channel: evaluation with Villermaux/Dushman test reaction. Microsystem Technologies 23: 3117–3130. https://doi.org/10.1007/s00542-016-3118-6

[20] Kakavandi FH, Rahimi M, Jafari O, Azimi N (2016) Liquid–liquid two-phase mass transfer in T-type micromixers with different junctions and cylindrical pits. Chemical Engineering and Processing 107: 58–67. https://doi.org/10.1016/j.cep.2016.06.011

[21] Karami E, Rahimi M, Azimi N (2018) Convective heat transfer enhancement in a pitted microchannel by stimulation of magnetic nanoparticles. Chemical Engineering and Processing 126: 156–167. https://doi.org/10.1016/j.cep.2018.02.023

[22] Yao C, Zhao Y, Ma H, Liu Y, Zhao Q, Chen G (2021) Two-phase flow and mass transfer in microchannels: A review from local mechanism to global models. Chemical Engineering Science 229: 116017. https://doi.org/10.1016/j.ces.2020.116017

[23] Constantinou A, Ghiotto F, Lam KF, Gavriilidis A (2014) Stripping of acetone from water with microfabricated and membrane gas–liquid contactors. Analyst 139: 266–272. https://doi.org/10.1039/C3AN00963G

[24] Davidy A (2023) CFD simulation of hydrogen sulfide (H_2S) desulfurization using ionic liquids and graphene oxide membrane. Fuels 4(3): 363–375. https://doi.org/10.3390/fuels4030023

[25] Sun W, Cao X, Yang W, Zhao X (2018) CFD modeling on non-equilibrium condensation process of H_2S in CH_4–H_2S mixture expansion through supersonic nozzles. Fuel Processing Technology 170: 53–63. https://doi.org/10.1016/j.fuproc.2017.10.002

[26] Mando M (2019) CFD simulation of H_2S scavenger injection. M.Sc. Thesis, Aalborg University, Esbjerg, Denmark.

[27] Almasvandi MH, Rahimi M, Tagheie Y (2016) Microfluidic cold stripping of H_2S from crude oil in low temperature and natural gas consumption. Journal of Natural Gas Science and Engineering 34: 499–508. https://doi.org/10.1016/j.jngse.2016.07.021

[28] Pan MY, Li T, Zhou Y, Qian Z, Shao L, Wang JX, Chen JF (2015) Selective absorption of H_2S from a gas mixture with CO_2 in a microporous tube-in-tube microchannel reactor. Chemical Engineering and Processing 95: 135–142. https://doi.org/10.1016/j.cep.2015.06.008

[29] Chen Y, Wang Y, Yan Z, Deng J, Luo G (2023) Selective removal of H_2S over CO_2 in a membrane gas–liquid microdispersion microreactor. Separation and Purification Technology 314: 123600. https://doi.org/10.1016/j.seppur.2023.123600

[30] Li X, et al. (2023) Machine learning-assisted CFD prediction of H_2S removal by deep eutectic solvents. Separation and Purification Technology. https://doi.org/10.1016/j.seppur.2023.124472

[31] Tran LT, et al. (2024) CFD-based optimization of high-gravity rotating packed bed for H_2S and CO_2 removal. Chemical Engineering Journal. https://doi.org/10.1515/chem-2020-0187

[32] Fluent Inc. (2006) FLUENT 6.3 User's Manual. Centera Resource Park, 10 Cavendish Court, Lebanon, NH, USA